ResearchGate

See discussions, stats, and author profiles for this publication at: https://www.researchgate.net/publication/263942905

Carbonated Nano Hydroxyapatite Crystal Growth Modulated by Poly(ethylene glycol) with Different Molecular Weights

ARTICLE *in* CRYSTAL GROWTH & DESIGN · APRIL 2012

Impact Factor: 4.89 · DOI: 10.1021/cg200917y

CITATIONS
11

READS
18

4 AUTHORS, INCLUDING:

Huaifa Zhang
McGill University
3 PUBLICATIONS **28** CITATIONS
SEE PROFILE

Ming Liu
Cincinnati Children's Hospital Medical Center
259 PUBLICATIONS **2,696** CITATIONS
SEE PROFILE

Hongsong Fan
Sichuan University
71 PUBLICATIONS **1,099** CITATIONS
SEE PROFILE

Available from: Huaifa Zhang
Retrieved on: 02 February 2016

CRYSTAL GROWTH & DESIGN

Article

pubs.acs.org/crystal

Carbonated Nano Hydroxyapatite Crystal Growth Modulated by Poly(ethylene glycol) with Different Molecular Weights

Huaifa Zhang,[†] Ming Liu,*[,‡] Hongsong Fan,*[,†] and Xingdong Zhang[†]

[†]National Engineering Research Center for Biomaterials and [‡]Analytical & Testing Center, Sichuan University, Chengdu 610064, Sichuan, China

Supporting Information

ABSTRACT: The effects of poly(ethylene glycol) (PEG) molecular weights on nano hydroxyapatite (n-HA) crystal growth were studied, and a possible mechanism was proposed. n-HA crystals were synthesized in the presence of PEG with different molecular weights via hydrothermal method. Transmission electron microscopy (TEM) analysis showed that the presence of PEG increased the size of n-HA crystals; PEG with larger molecular weights produced larger n-HA crystals. High-resolution TEM observation indicated that all of the n-HA crystals tended to grow along the ⟨002⟩ axis. X-ray diffraction patterns showed that all of the samples consisted of only the HA phase. Besides, PEG increased the crystallinity of n-HA crystals, and this effect was more significant for PEGs with larger molecular weights. Fourier transform infrared results further revealed that all of the crystals were carbonated HA. Thermogravimetry/differential scanning calorimetry analysis detected PEG residues on n-HA particles. To thoroughly study the modulating mechanism of PEGs on n-HA crystal growth, n-HA samples heat-treated for various times were prepared in the presence of PEG20000, and a possible mechanism in which PEG modulated the growth of n-HA crystals was discussed.

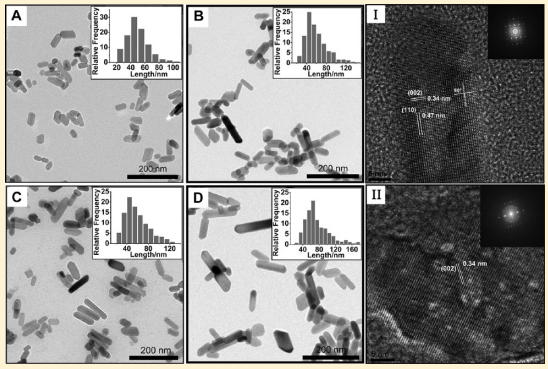

1. INTRODUCTION

Hydroxyapatite (HA) is chemically compatible with the inorganic phase of natural bone[1] and has been widely used in the field of biomaterials.[2−4] Nevertheless, the mineral phases in natural bones are nonstoichiometric HA with an average size of 25 nm in width and 50 nm in length, containing impurities including carbonate, chloride, fluoride, and magnesium.[5−9] Moreover, the formation of natural bones is a biomineralization process, in which both nucleation and growth of the mineral crystals occur in the presence of organic macromolecules. The functional groups in the organic molecules play an important role in mediating the size, morphology, and chemistry of the mineral crystals in in vivo systems.[5,10]

Inspired by biomineralization, it has been widely accepted that organic molecules can manipulate the growth of HA crystals.[5,11−14] To date, extensive research has been done to investigate the effects of organic molecules on HA crystal growth. The results showed that a variety of polymers, including amino acids,[14,15] hyaluronic acid,[16] polyvinylpyrrolidone (PVP),[17] sodium dodecyl sulfonate (SDS),[18] and ethylene diamine tetraacetic acid (EDTA),[19] indeed affected the growth behavior of HA crystals and eventually influenced their morphologies. Recently, some researchers found that poly(ethylene glycol) (PEG) also affected HA formation,[20−22] which is meaningful for the study of HA crystal growth modulated by organic molecules.

PEG is completely composed of ethylene oxygen groups ($-CH_2-CH_2-O-$) and has been widely used in biomedical research and applications.[23,24] PEGs of different molecular weights have attracted intensive interest in drug delivery systems[24−26] and bone tissue engineering.[27,28] When PEGs with different molecular weights are introduced into in vivo systems, they depart from the drug delivery vehicles[29] or scaffolds[30] and may participate into biomineralization. Therefore, investigation of the effects of PEGs on HA crystal growth might give some clues to the understanding of the interactions between PEG implants and natural tissues.

Qiu et al.[20] investigated the influence of PEG6000 on n-HA morphology. They found that PEG6000 changed HA morphology and that this effect varied with PEG6000 concentrations. Another study reported that PEG600 induced the axis orientation growth of HA crystals under hydrothermal conditions via interactions between the ether bonds of PEG600 and HA crystals.[22] Although they all confirm that PEG affects HA crystal morphology, the growth process of HA in the presence of PEG is still unclear. Besides, PEGs with different molecular weights were employed in the literature, but a systemic study of the influence of PEG molecular weight on HA growth is rarely touched. Researchers have found that PEG molecular weight can influence crystal morphology of calcium carbonate and LiV_3O_8;[31,32] hence, it is reasonable to suspect that PEG molecular weight may also affect HA crystal growth.

Received: July 17, 2011
Revised: March 7, 2012
Published: March 21, 2012

ACS Publications © 2012 American Chemical Society

To systematically investigate the influence of PEG on n-HA crystal growth, it is important to select a proper method to synthesize HA. Till now, HA has been synthesized by different routes, such as chemical precipitation,[7,17] sol−gel synthesis,[33−35] spray pyrolysis synthesis,[36] mechanochemical synthesis,[37−39] and mechanochemical-hydrothermal reaction.[40,41] Nevertheless, these methods are either time-consuming,[17,20] producing poorly dispersed or irregular crystals,[35,36,42] or demanding expensive facilities.[36] Unlike those methods, the hydrothermal technique is an efficient approach to synthesize crystals with distinct morphological features and good dispersivity,[43,44] making it convenient to examine the dimensions of the obtained particles. Hence, the hydrothermal technique is a good candidate to investigate the morphological changes of HA crystals in the presence of PEGs.

Therefore, the present work aimed to investigate the effects of PEG molecular weight on n-HA crystals using the hydrothermal method. The influence of PEGs on n-HA crystal growth process was probed as well, using PEG20000 as a model polymer. Finally, a possible mechanism in which PEGs modulate n-HA crystals growth was proposed.

2. EXPERIMENTAL SECTION

2.1. Reagents. PEG (PEG400, M_w = 400, polydispersity index = 1.06; PEG6000, M_w = 6000, polydispersity index = 1.06; and PEG20000, M_w = 20000, polydispersity index = 1.05) (AR), $(NH_4)_2HPO_4$ (AR), $Ca(NO_3)_2{\cdot}4H_2O$ (AR), and $NH_3{\cdot}H_2O$ (AR) were purchased from Chengdu Kelong Chemical Reagent Factory, China, and were used as the initial chemicals.

2.2. Synthesis of n-HA. Typically, an equal volume of 0.06 mol/L $(NH_4)_2HPO_4$ aqueous solution was added drop by drop into 0.1 mol/L $Ca(NO_3)_2$ aqueous solution while being stirred, and the pH was maintained at 11.0 by adding $NH_3{\cdot}H_2O$. When the addition of $(NH_4)_2HPO_4$ was finished, the obtained milky solution was further stirred for 30 min. All of the above processes were carried out at 1 °C. After that, the precursor solution was transferred to a Teflon-lined autoclave container and heat-treated at 150 °C for 40 h. The as-prepared sample was referred to as control-40. The obtained precipitates were collected and washed five times with deionized water by centrifugation before subsequent analysis. During the washing process, the precipitates were treated with ultrasound for 10 min before centrifugation each time. Finally, the washed precipitates were either dried at 60 °C or redispersed in ethanol by ultrasound.

To investigate the effects of PEG molecular weight on n-HA, PEG400, PEG6000, and PEG20000 were dissolved, respectively, in the aqueous solution of 0.1 mol/L $Ca(NO_3)_2$ first, and the concentration of the PEGs in $Ca(NO_3)_2$ was designed to be 16 wt % (about 8 wt % in the reaction system). Then, subsequent experiment steps like control-40 were performed. Similarly, these samples were referred to as PEG400-40, PEG6000-40, and PEG20000-40, respectively.

To accurately understand the growth process of n-HA crystals in the presence of PEGs, extra samples heat-treated for various times were synthesized. In such experiments, PEG20000 was employed as a model polymer, and similar experimental processes with PEG20000-40 were carried out except that the heat treatment times were 4 and 15 h. The synthesized samples were referred to as PEG20000-4 and PEG20000-15. Control experiments without PEG20000 were also performed following the same method, and the obtained samples were referred to as control-4 and control-15.

2.3. Test of Electrical Conductivity (EC) of the $Ca(NO_3)_2$ Solution. The EC of the $Ca(NO_3)_2$ solution was measured by a Mettler Toledo FE30 conductometer before and after the addition of PEGs, and the EC changes were calculated. For the $Ca(NO_3)_2$-PEG solutions, the EC was measured 10 min after complete dissolution of the PEGs.

2.4.1. Characterization of n-HA. *TEM (Transmission Electron Microscopy).* Both size and morphology of the products were characterized using a Tecnai G^2 F20 S-TWIN TEM. High-resolution TEM (HRTEM) was recorded to investigate the microstructure of the crystals. The samples dispersed in ethanol were used for TEM test. Image-Pro Plus (Ver 6.0, Media Cybernetics)[45] was employed to analyze the size of the crystals from TEM micrographs. More than 350 individual crystals were measured for each sample to obtain their mean size and size distribution. Student's t test was used to determine the significant difference of the samples. The significant difference was determined when the probability was $P < 0.05$.

2.4.2. XRD (X-ray Diffraction). Phase composition and crystallinity of the dried samples were investigated by XRD employing a Dandong Fangyuan DX-1000 diffractometer in the 2θ range of 4−70° using Cu Kα radiation. Jade processing software (Ver 5.0, Materials Data, Inc.)[46,47] was used to analyze phase composition and crystallinity of the samples. XRD tests were conducted three times for each sample. Student's t test was used to determine the significant difference of the samples in crystallinity, which was determined when the probability was $P < 0.05$.

2.4.3. FTIR (Fourier Transform Infrared Test). FTIR spectra were obtained using a Perkin-Elmer Spectrum one (B) spectrometer to inspect function group composition of the samples.

2.4.4. TG/DSC (Thermogravimetry/Differential Scanning Calorimetry). To verify the chemical composition of the crystals, TG/DSC analysis of PEG20000, control-40, and PEG20000-40 was performed on Netzsch STA 449 C at 10 °C/min in a nitrogen flow of 30 mL/min in alumina crucibles.

3. RESULTS AND DISCUSSION

3.1. Effects of PEGs on the EC of $Ca(NO_3)_2$ Solution. Table 1 shows EC results of the $Ca(NO_3)_2$ solutions. The EC

Table 1. EC Decreases of $Ca(NO_3)_2$-PEG Solutions

	16 wt %		
	PEG400-$Ca(NO_3)_2$	PEG6000-$Ca(NO_3)_2$	PEG20000-$Ca(NO_3)_2$
EC of $Ca(NO_3)_2$ (mS/cm)	15.25 ± 0.008	15.26 ± 0.012	15.25 ± 0.010
EC of $Ca(NO_3)_2$-PEG (mS/cm)	9.15 ± 0.028	9.10 ± 0.061	9.105 ± 0.007
decreased EC(mS/cm)	6.10	6.16	6.15

of the $Ca(NO_3)_2$ solution decreased after the addition of PEGs, but the EC changes for all of the $Ca(NO_3)_2$-PEG solutions were almost the same. The EC of the $Ca(NO_3)_2$ solutions decreased because PEG interacted with Ca^{2+} ions[48] and trapped them, reducing the amount of free Ca^{2+} in solution. All of the $Ca(NO_3)_2$-PEG solutions underwent almost the same EC decreases possibly because the fundamental unit interacting with Ca^{2+} ions in the PEG chains was $-CH_2-CH_2-O-$.[48] Given that the same amount of PEG was added, the numbers of $-CH_2-CH_2-O-$ were also the same in all of the $Ca(NO_3)_2$-PEG solutions. Consequently, the same number of Ca^{2+} ions was trapped, resulting in the same EC changes.

3.2.1. Effect of PEG Molecular Weight on n-HA. *XRD Results.* Figure 1 shows XRD patterns of the samples. All of the XRD patterns fitted well with the International Centre for Diffraction Data (ICDD) database PDF#09-0432, suggesting that all of the prepared samples were pure HA without any other calcium phosphate (CaP) phases. The crystallinity of the HA crystals was calculated employing the following equation:[47]

$$M = \frac{I'}{I}$$

dx.doi.org/10.1021/cg200917y | Cryst. Growth Des. 2012, 12, 2204−2212

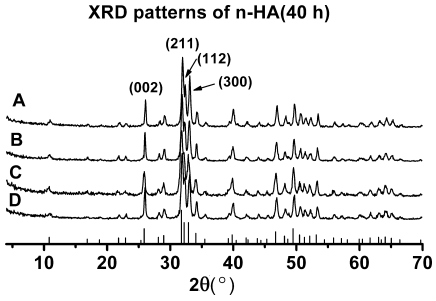

Figure 1. XRD patterns of the as-prepared samples in the presence of PEGs: (A) PEG20000-40, (B) PEG6000-40, (C) PEG400-40, and (D) control-40.

where M was the crystallinity, I' was the intensity of crystalline portion, and I was the total intensity of crystalline and noncrystalline portion. I' and I were determined by Jade software. Background scattering was removed before crystallinity calculation, using the BG function (cubic spline, strip K-α2-K-α1/α2 ratio 2.0) of Jade software. The calculated average crystallinity of control-40, PEG400-40, PEG6000-40, and PEG20000-40 was 88.3, 88.8, 92.0, and 92.1%, respectively. t test results show that the cyrstallinity of PEG20000-40 and PEG6000-40 was significantly larger than that of control-40 and PEG400-40 (Figure S1 in the Supporting Information). These results indicate that the addition of PEGs increased the crystallinity of the samples and that PEGs with larger molecular weights had bigger effects. The possible reason will be discussed in section 3.4.

3.2.2. FTIR Spectra. FTIR spectra are shown in Figure S2 in the Supporting Information. The absorption bands at 1094, 1035, 960, 602, 561, and 473 cm^{-1} are characteristic PO_4^{3-} peaks.[4,49] The peaks at 3570 and 631 cm^{-1} are for −OH stretching vibration and libration, respectively.[50] The doublet peaks at 1460 and 1420 cm^{-1} as well as the peak at 875 cm^{-1} can be attributed to the vibrational frequencies of carbonate ions that substituted the phosphate,[51,52] indicating that all of the samples were carbonated HA. No characteristic PEG peaks were found in any of the samples. However, it does not mean that there was no PEG residue in the samples. This will be further proved by the TG/DSC results.

3.2.3. TG/DSC Curves. Figure 2 displays the TG/DSC results. Figure 2A shows that polymer PEG20000 mainly experienced three phases. The first phase that occurred around 77.1 °C was due to the melting of PEG20000. The second phase took place around 400 °C, which should correspond to PEG20000 decomposition. The last phase was recorded around 927.4 °C, which may be out of the phase transformation of carbon. Figure 2B,C reveals that the TG/DSC curves of control-40 and PEG20000-40 were different, and the latter experienced a larger weight loss. One possible reason could be that PEG20000 was not completely removed from PEG20000-40 during the washing process. On one hand, PEG20000-40 had more adsorbed water than control-40, as indicated by the endothermic curve of PEG20000-40 around 98.5 °C, while PEG20000 can absorb water by forming bonds with it,[53] so PEG20000-40 may have PEG20000 residues on the surface. On the other hand, the difference between the two TG/DSC curves ranging from 352 to 1200 °C also supports the above proposition. For control-40, the weight loss from 352 up to 1200 °C was out of the slow elimination of the carbonate groups in HA crystals. However, for PEG20000-40, the weight loss from 352 up to 1200 °C mainly should be the result of PEG20000 decomposition, accompanied by slow elimination of carbonate groups.[54] Especially, the endothermic curve of PEG20000-40 at 484.5 °C should be due to the decomposition of PEG20000 residue, as shown by the TG/DSC curve of PEG20000. The decomposition of PEG20000 generated C. The mass loss between 800 and 900 °C, accompanied with an endothermic peak, should be due to the reaction between C and H_2O from HA dehydration. HA started to dehydrate at 850 °C.[55] C reacted with H_2O at high temperatures and turned into gases, resulting in mass loss and an endothermic peak. Moreover, this reaction reduced the ambient humidity of HA, which promoted HA decomposition at high temperature.[55] Therefore, HA decomposed and produced α-TCP.[56] Between 900 and 1000 °C, α-TCP transferred into more stable β-TCP and generated an exothermic peak in this area.[57] The residue of

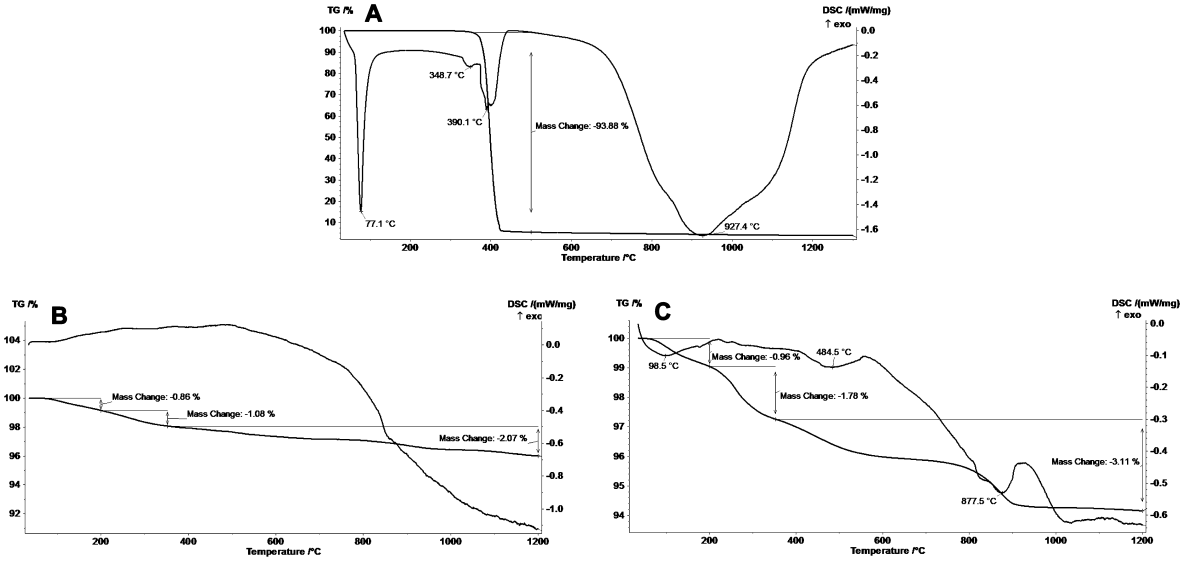

Figure 2. TG/DSC patterns of (A) PEG20000, (B) control-40, and (C) PEG20000-40.

dx.doi.org/10.1021/cg200917y | Cryst. Growth Des. 2012, 12, 2204−2212

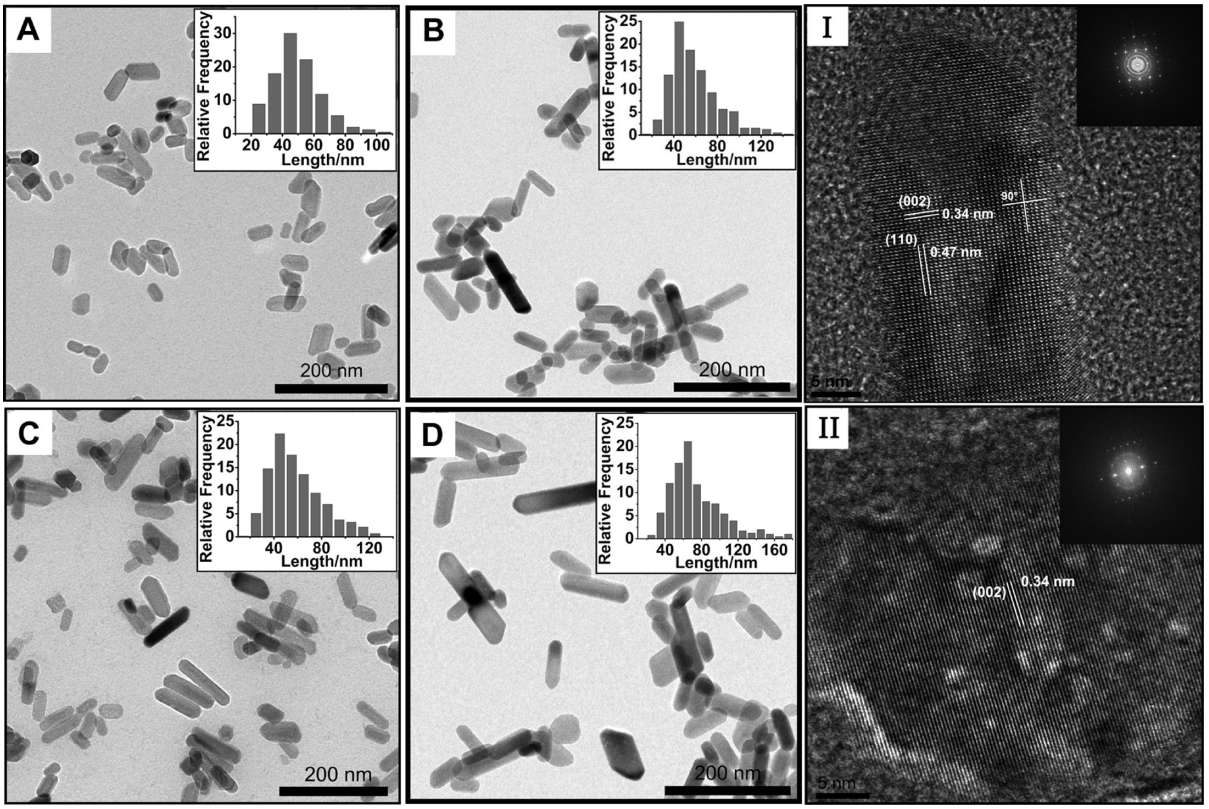

Figure 3. TEM pictures (left) of the n-HA crystals in the presence of PEGs: (A) control-40, (B) PEG400-40, (C) PEG6000-40, and (D) PEG20000-40. The inserts show the length distribution of the samples. HRTEM results (right): (I) control-40 and (II) PEG20000-40. The inserts are corresponding FFT patterns of the HRTEM fringes using the Digital Micrograph software.

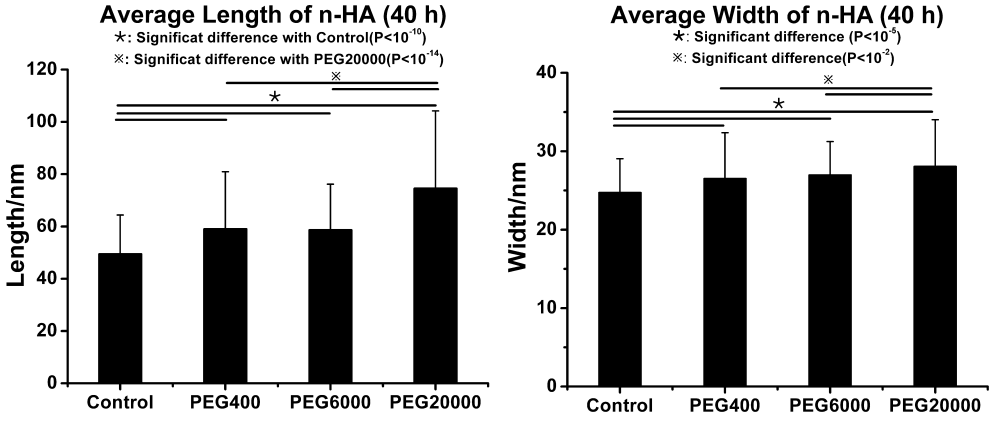

Figure 4. Average sizes of the n-HA crystals in the presence of PEGs calculated from the TEM micrographs.

PEG20000 on PEG20000-40 indicates that PEG20000 adsorbed onto HA crystals.

3.2.4. TEM and HRTEM Results. Figure 3 displays TEM and HRTEM results of the crystals prepared in the presence of the PEGs. According to Figure 3 (left), control-40 consisted of both suborbicular and sheetlike crystals, but all of the other samples were mainly sheetlike crystals. The inserted pictures show that crystal length distribution of the samples shifted toward larger sizes in the presence of PEGs. Moreover, this shift increased with the increase of PEG molecular weight. HRTEM results indicate that both control-40 and PEG20000-40 were single HA crystals and that n-HA crystals tended to grow along the ⟨002⟩ axis. Figure 4 shows average sizes of the as-prepared n-HA crystals calculated from the TEM micrographs. According to Figure 4, the presence of PEGs significantly increased the size of n-HA crystals, and the size changes depended on PEG molecular weights. Although there was no significant difference between the average size of PEG400-40 and that of PEG6000-40, PEG20000-40 had a significantly larger average size. Besides, PEGs increased the aspect ratio of the n-HA crystals (Table S1 in the Supporting Information). This effect was also PEG molecular weight-dependent, and PEG20000-40 had the largest aspect ratio. Therefore, it is reasonable to conclude that PEG molecular weight influenced the morphology and size of n-HA crystals and that the effects varied with molecular weights. These results may be due to the Ca^{2+} trapping effect of PEG as well as the

dx.doi.org/10.1021/cg200917y | *Cryst. Growth Des.* 2012, 12, 2204–2212

adsorption of PEG chains onto the n-HA crystals, which will be discussed in detail in section 3.4.

3.3.1. Growth Process of n-HA Crystal. *XRD Results of the Samples Heat-Treated for Various Times.* Figure 5 shows

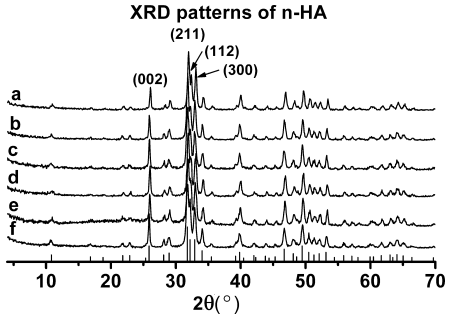

Figure 5. XRD patterns of the as-prepared HA crystals with different heat treatment times: (a) PEG20000-40, (b) PEG20000-15, (c) PEG20000-4, (d) control-40, (e) control-15, and (f) control-4.

XRD patterns of the samples heat-treated for various times. The XRD patterns indicate that all of the crystals consisted of only HA phase. The average crystallinity of control-4, control-15, control-40, PEG20000-4, PEG20000-15, and PEG20000-40 was 87.5, 87.2, 88.3, 89.7, 91.7, and 92.1%, respectively. These results show that the crystallinity of the samples increased with the heat treatment time except for control-15. Besides, the crystallinity of PEG20000-15 and PEG20000-40 was significantly higher than that of control-15 and control-40, respectively (Figure S3 in the Supporting Information). Therefore, the presence of PEG20000 influenced HA growth and increased the crystallinity of HA crystals. The possible reason will be discussed in section 3.4.

3.3.2. TEM Results of the Samples Heat-Treated for Various Times. Figure 6 shows the TEM pictures of the as-prepared n-HA crystals heat-treated for various times. All of the control samples consisted of both suborbicular and sheetlike crystals. PEG20000-4 also consisted of both suborbicular and sheetlike crystals, while PEG20000-15 and PEG20000-40 mainly consisted of sheetlike crystals. The inserted length distribution pictures reveal that the length distribution of all of the n-HA samples moved to larger scales when they were heat-treated for longer times. More than that, the addition of PEG20000 resulted in longer crystals as compared to control samples under the same conditions, except for the samples heat-treated for 4 h. This phenomenon agrees with the calculated average length of the crystals shown in Figure 7 (left). As shown in Figure 7, the average length of the control samples increased when the heat treatment time increased to 15 h but then did not undergo significant changes when the heat treatment time increased to 40 h. On the contrary, both average length and width of the as-prepared n-HA crystals kept increasing significantly with the increase of heat treatment time in the presence of PEG20000. In addition, samples with PEG20000 always had larger crystal sizes than control samples under the same conditions. Therefore, the addition of PEG20000 did modulate the growth process of n-HA crystals, changed n-HA morphology, and increased n-HA size. The possible modulating mechanism will be discussed later.

3.4. Mechanism of the PEG Modulation of n-HA Crystal Growth. All of the above experimental results reveal first that the synthetic method used in this work was effective to

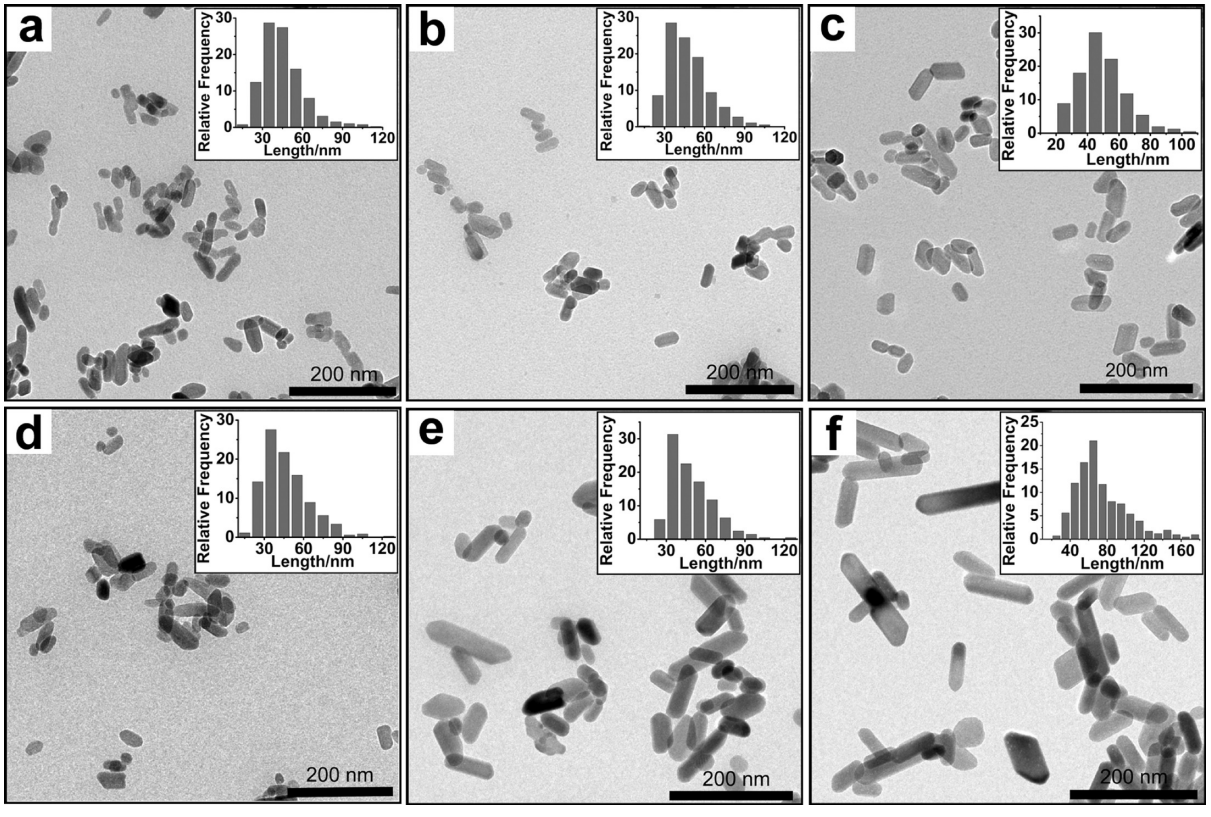

Figure 6. TEM pictures of the as-prepared n-HA crystals with different heat treatment times: (a) control-4, (b) control-15, (c) control-40, (d) PEG20000-4, (e) PEG20000-15, and (f) PEG20000-40. The inserts show the length distribution of the samples.

dx.doi.org/10.1021/cg200917y | Cryst. Growth Des. 2012, 12, 2204–2212

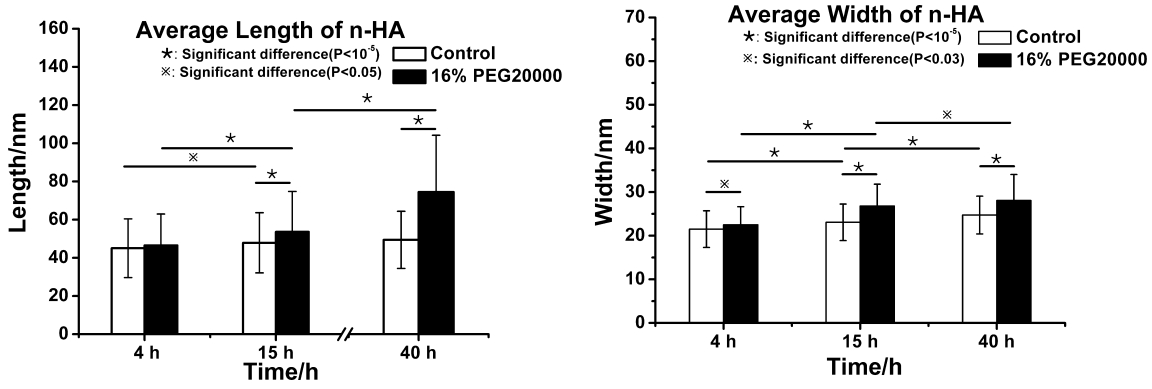

Figure 7. Average sizes of the as-prepared n-HA crystals with different heat treatment times, calculated from the TEM micrographs.

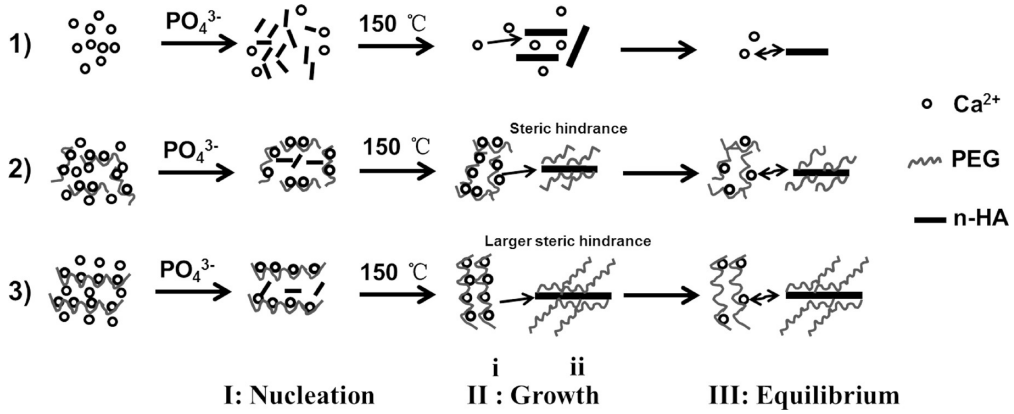

Figure 8. Proposed n-HA crystal growth mechanism: (1) control, (2) short PEG chain, and (3) long PEG chain.

get n-HA with good dispersivity and further investigate the influence of PEG on n-HA growth process. In Qiu's report,[20] a special wet precipitate method was used, but no data about size distribution were available, possibly due to poor dispersivity of the prepared HA particles. To obtain n-HA particles with good dispersivity and distinguish shapes, the hydrothermal method was employed following the initial precipitation of n-HA at a low temperature. As low reaction temperature prior to hydrothermal treatment can reduce n-HA size,[58] reactions were first carried out at 1 °C to get smaller n-HA. High pH conditions (pH = 11.0) were employed to promote the formation of HA during heat treatment. The heat treatment temperature of 150 °C was selected according to Wang's work[22] where 100 and 200 °C were used to get rodlike n-HA particles. According to our preliminary experiments, n-HA stopped growing after being heat-treated for 40 h, so 40 h was used as the longest heat treatment time. Qiu's research indicated that higher PEG concentrations had larger influence on n-HA growth.[20] Hence, a PEG concentration of 8 wt % in the reaction system, which was close to the highest PEG concentration used in Qiu's experiments, was used to obtain more significant results.

On the basis of the above synthetic conditions, together with PEGs of various molecular weights and different heat treatment times, a series of n-HA particles with different morphologies and sizes were prepared. The effects of PEG as well as PEG molecular weight on HA crystal growth were confirmed. In view of these experimental results, a possible growth mechanism of n-HA crystals in the presence of PEG is illustrated in Figure 8. The whole process includes three stages: nucleation (stage I), growth of crystals (stage II), and finally an equilibrium state (stage III).

At the early stage, a large amount of crystals was formed from the highly supersaturated precursor solution [Figure 8 (stage I)]. Because the reaction was so fast, the effects of PEG on n-HA crystal growth were not obvious in this stage. Hence, the crystals of control-4 and PEG20000-4 had similar morphologies and crystallinity (Figures 6 and S3 in the Supporting Information).

As the heat treatment time increased, the effects of PEG on n-HA crystal growth became more obvious as compared with control. The presence of PEGs changed the n-HA morphology, increased the n-HA crystal size, and modulated the n-HA growth process. The role of PEG could be interpreted from two aspects [Figure 8 (stage II)].

On the one hand, PEG interacted with Ca^{2+} ions and trapped them [Figure 8 (stage II-i)], as evidenced by the EC results. Because of the trapping effect, the number of initial nucleating centers formed at stage I was reduced, leaving more Ca^{2+} ions to facilitate n-HA crystal growth in the subsequent heat-treating process, and thus, larger n-HA crystals were produced in the presence of PEGs (Figures 3, 4, 6, and 7). Through the trapping effect, PEG also slowed down the incorporation speed of Ca^{2+} ions into the n-HA crystals, making it take a longer time to achieve an equilibrium state, and thus, the n-HA crystals kept growing as the heat treatment time increased (Figure 6). In contrast, the control samples stopped growing after being heat-treated for 15 h due to their high reaction speed. This was consistent with Qiu's study,[20] in which they also concluded that PEG chelated Ca^{2+} and restrained HA formation. In addition, the slower incorporation speed of Ca^{2+} ions into n-HA crystals

dx.doi.org/10.1021/cg200917y | Cryst. Growth Des. 2012, 12, 2204−2212

could also make Ca^{2+} ions deposit more regularly onto n-HA crystals, resulting in higher crystal crystallinity in the presence of PEGs, which was proved by the XRD results (Figures 1 and 5). This phenomenon became more obvious as the reaction time increased (Figure 5). Because HA has a preferred growth orientation along *c*-axis (Figure 3), limited Ca^{2+} ions escaped from PEG chains would preferentially deposit on the growth face along the *c* direction. Therefore, the as-prepared crystals would be longer than control particles, as was proved by Figures 3 and 6 and Table S1 in the Supporting Information. In short, through interacting with Ca^{2+}, PEG slowed down n-HA formation, increased n-HA crystallinity, and favored n-HA growth.

On the other hand, PEG adsorbed onto the surface of the crystals[17,48] [Figure 8 (stage II-ii)], as proved by TG/DSC results. The adsorption of PEG onto the crystal surfaces might further promote the crystals to grow along the *c*-axis, resulting in longer n-HA crystals, as shown in Figures 3 and 6. This was consistent with Wang's report,[22] who also proposed that PEG600 induced axis orientation growth of HA through interacting with HA crystals. Xie et al.[32] found that PEG molecular weight influenced calcium carbonate crystal structure, and high molecular weight PEG favored calcite formation. In their opinion, PEG stabilized calcium carbonate crystals by binding to certain faces of the crystals and changed the faces' growth rates, but high molecular weight PEGs would increase solution viscosity, so their stabilization effect might be reduced, and thus, calcite was generated in the presence of higher molecular weight PEGs.[32] Obviously, their explanation is not suitable here. We think this is because HA and calcium carbonate have different crystal structures. In our study, after the initial precipitate at low temperature (1 °C), a post-heat treatment (150 °C) was applied. Hence, nonspherical n-HA crystals with good crystalline were formed in a short time. This was very different from Qiu's report[20] in which spherical particles were produced. This difference may come from their special precipitate process in which room temperature was applied together with extremely slow reaction speed (it took 5 days to finish the reaction). According to the literature, a high-temperature heat treatment was more likely to produce crystalline HA with preferred growth direction.[59−61] This initially formed n-HA crystals that had a very obvious aspect, and it is difficult to change their basic growth direction, so the subsequent growing process continued based on it. Consequently, the variation of solution viscosity could be ignored. Because there are more Ca^{2+} on the lateral faces[62] and there is also more space on them, the PEG molecule chains adsorbed to HA were more likely to bind along these faces as shown in Figure 8 (stage II). The adsorbed PEG chains reduced the following Ca^{2+} precipitation on these faces by steric hindrance and promoted *c*-axis growth (Figures 3, 4, 6, and 7). A longer molecule PEG chain might show larger steric hindrance against Ca^{2+} ions' precipitation on these faces; therefore, the crystal growth was more favored along the *c*-axis. As a result, PEG20000-40 experienced more increase in length but relatively less increase in width and gained the largest aspect ratio (Table S1 in the Supporting Information). Moreover, the larger steric hindrance from longer PEG chains may also make the Ca^{2+} deposit more regularly onto the crystals and, therefore, increased the crystal crystallinity (Figure 1).

Finally, when the reaction system reached the dynamic equilibrium state [Figure 8 (stage III)], the n-HA crystals would stop growing. In sum, the PEG modulation of n-HA growth is a combined result of Ca^{2+} trapping and surface adsorption effects of PEG; the larger effects of higher molecular weight PEGs on n-HA growth may be due to their larger steric hindrance.

From the previous description, we can see that PEG modulates n-HA growth through the combination of its Ca^{2+} trapping and surface adsorption effects; higher molecular weight PEGs had larger effects on n-HA growth because their longer chains produced larger steric hindrance, making Ca^{2+} deposit more regularly into the crystals. The way that PEG molecules modulate HA crystal growth may give us some clues to prepare inorganic crystals with desired morphology and/or size. According to the literature, many organic molecules serve as templates to modulate HA growth.[18,63−65] Here, we found that the size and morphology of HA were also affected by the polymer−Ca^{2+} interaction and the surface adsorption of polymer chains, which change the ion deposition speed into the crystals and the ion deposition priorities on different crystal faces, respectively. Therefore, this work provides more options for us to prepare HA crystals with different sizes and morphologies.

4. CONCLUSIONS

n-HA crystals assembling the shape and chemical composition of natural bone minerals were synthesized and modulated by PEGs. The experimental results indicate that PEG molecular weight had a significant influence on both the size and the crystallinity of n-HA crystals and that PEGs with larger molecular weights had larger effects. The presence of PEG affected n-HA crystal growth kinetics as well. On the basis of the experiment results, a possible mechanism in which PEG modulated n-HA crystal growth was proposed. Out of its Ca^{2+} trapping effect as well as the adsorption effect, PEG promoted the growth of n-HA crystals and also increased the crystal crystallinity. In conclusion, PEG molecular weight significantly influenced both the size and the crystallinity of n-HA crystals by modulating the growth process of n-HA.

■ ASSOCIATED CONTENT

Ⓢ Supporting Information

Significant difference results about the crystallinity of the samples in Figures 1 and 5, FTIR spectra of the as-prepared samples in the presence of PEGs, FTIR spectra of the as-prepared samples with different heat treatment times, statistical analysis method of n-HA size, and the raw data of the XRD patterns in Figures 1 and 5 after background scattering subtraction. This material is available free of charge via the Internet at http://pubs.acs.org.

■ AUTHOR INFORMATION

Corresponding Author

*E-mail: mingliu@scu.edu.cn (M.L.) or hsfan@scu.edu.cn (H.F.).

Notes

The authors declare no competing financial interest.

■ ACKNOWLEDGMENTS

We are thankful for the financial support from National Natural Science Foundation of China (Contract Grant No. 81071272) and National Basic Research Program of China (Contract Grant No. 2011CB606201).

REFERENCES

(1) Young, R. Implications of atomic substitutions and other structural details in apatites. *J. Dent. Res.* **1974**, *53* (2), 193.

(2) Kester, M.; Heakal, Y.; Fox, T.; Sharma, A.; Robertson, G. P.; Morgan, T. T.; Altinoğlu, E. I.; Tabakovic, A.; Parette, M. R.; Rouse, S. M.; Ruiz-Velasco, V.; Adair, J. H. Calcium Phosphate Nanocomposite Particles for In Vitro Imaging and Encapsulated Chemotherapeutic Drug Delivery to Cancer Cells. *Nano Lett.* **2008**, *8* (12), 4116−4121.

(3) Schwiertz, J.; Wiehe, A.; Gräfe, S.; Gitter, B.; Epple, M. Calcium phosphate nanoparticles as efficient carriers for photodynamic therapy against cells and bacteria. *Biomaterials* **2009**, *30* (19), 3324−3331.

(4) Joseph Nathanael, A.; Mangalaraj, D.; Chi Chen, P.; Ponpandian, N. Enhanced mechanical strength of hydroxyapatite nanorods reinforced with polyethylene. *J. Nanopart. Res.* **2011**, *13* (5), 1841−1853.

(5) Boskey, A. L. Mineralization of Bones and Teeth. *Elements* **2007**, *3* (6), 385−391.

(6) Ferraz, M. P.; Monteiro, F. J.; Manuel, C. M. Hydroxyapatite nanoparticles: A review of preparation methodologies. *J. Appl. Biomater. Biomech.* **2004**, *2* (2), 74−80.

(7) Palmer, L. C.; Newcomb, C. J.; Kaltz, S. R.; Spoerke, E. D.; Stupp, S. I. Biomimetic systems for hydroxyapatite mineralization inspired by bone and enamel. *Chem. Rev.* **2008**, *108* (11), 4754−4783.

(8) Tadic, D.; Peters, F.; Epple, M. Continuous synthesis of amorphous carbonated apatites. *Biomaterials* **2002**, *23* (12), 2553−2559.

(9) Vallet-Regí, M.; González-Calbet, J. M. Calcium phosphates as substitution of bone tissues. *Prog. Solid State Chem.* **2004**, *32* (1−2), 1−31.

(10) C lfen, H. Biomineralization: A crystal-clear view. *Nat. Mater.* **2010**, *9* (12), 960−961.

(11) Fratzl, P.; Gupta, H. S.; Paschalis, E. P.; Roschger, P. Structure and mechanical quality of the collagen-mineral nano-composite in bone. *J. Mater. Chem.* **2004**, *14* (14), 2115−2123.

(12) Stupp, S.; Braun, P. Molecular manipulation of microstructures: Biomaterials, ceramics, and semiconductors. *Science* **1997**, *277* (5330), 1242.

(13) De Yoreo, J.; Vekilov, P. Principles of crystal nucleation and growth. *Rev. Mineral. Geochem.* **2003**, *54* (1), 57.

(14) Zhang, H. G.; Zhu, Q.; Wang, Y. Morphologically Controlled Synthesis of Hydroxyapatite with Partial Substitution of Fluorine. *Chem. Mater.* **2005**, *17* (23), 5824−5830.

(15) Zhang, G.; Chen, J.; Yang, S.; Yu, Q.; Wang, Z.; Zhang, Q. Preparation of amino-acid-regulated hydroxyapatite particles by hydrothermal method. *Mater. Lett.* **2011**, *65* (3), 572−574.

(16) Chen, Z.; Zhou, H.; Wang, X.; Sang, L.; Wang, C.; Ma, J.; Li, X. Controlled mineralization by extracellular matrix: Monodisperse, colloidally stable calcium phosphate-hyaluronan hybrid nanospheres. *Chem. Commun.* **2010**, *46* (8), 1278−1280.

(17) Zhang, Y.; Lu, J. A Mild and Efficient Biomimetic Synthesis of Rodlike Hydroxyapatite Particles with a High Aspect Ratio Using Polyvinylpyrrolidone As Capping Agent. *Cryst. Growth Des.* **2008**, *8* (7), 2101−2107.

(18) Liu, C.; Ji, X.; Cheng, G. Template synthesis and characterization of highly ordered lamellar hydroxyapatite. *Appl. Surf. Sci.* **2007**, *253* (16), 6840−6843.

(19) Salarian, M.; Solati-Hashjin, M.; Shafiei, S. S.; Salarian, R.; Nemati, Z. A. Template-directed hydrothermal synthesis of dandelion-like hydroxyapatite in the presence of cetyltrimethylammonium bromide and polyethylene glycol. *Ceram. Int.* **2009**, *35* (7), 2563−2569.

(20) Qiu, C.; Xiao, X.; Liu, R. Biomimetic synthesis of spherical nano-hydroxyapatite in the presence of polyethylene glycol. *Ceram. Int.* **2008**, *34* (7), 1747−1751.

(21) Li, Y.; Weng, W. In vitro synthesis and characterization of amorphous calcium phosphates with various Ca/P atomic ratios. *J. Mater. Sci.: Mater. Med.* **2007**, *18* (12), 2303−2308.

(22) Wang, A.; Yin, H.; Liu, D.; Wu, H.; Wada, Y.; Ren, M.; Xu, Y.; Jiang, T.; Cheng, X. Effects of organic modifiers on the size-controlled synthesis of hydroxyapatite nanorods. *Appl. Surf. Sci.* **2007**, *253* (6), 3311−3316.

(23) Herold, D. A.; Keil, K.; Bruns, D. E. Oxidation of polyethylene glycols by alcohol dehydrogenase. *Biochem. Pharmacol.* **1989**, *38* (1), 73−76.

(24) Veronese, F. M.; Pasut, G. PEGylation, successful approach to drug delivery. *Drug Discovery Today* **2005**, *10* (21), 1451−1458.

(25) Huang, F. W.; Wang, H. Y.; Li, C.; Wang, H. F.; Sun, Y. X.; Feng, J.; Zhang, X. Z.; Zhuo, R. X. PEGylated PEI-based biodegradable polymers as non-viral gene vectors. *Acta Biomater.* **2010**, *6* (11), 4285−4295.

(26) Bailon, P.; Won, C. PEG-modified biopharmaceuticals. *Expert Opin. Drug Delivery* **2009**, *6* (1), 1−16.

(27) Bryant, S.; Anseth, K. Controlling the spatial distribution of ECM components in degradable PEG hydrogels for tissue engineering cartilage. *J. Biomed. Mater. Res., Part A* **2003**, *64* (1), 70−79.

(28) Burdick, J. A.; Anseth, K. S. Photoencapsulation of osteoblasts in injectable RGD-modified PEG hydrogels for bone tissue engineering. *Biomaterials* **2002**, *23* (22), 4315−4323.

(29) Hamidi, M.; Azadi, A.; Rafiei, P. Pharmacokinetic consequences of pegylation. *Drug Delivery* **2006**, *13* (6), 399−409.

(30) Burdick, J. A.; Mason, M. N.; Hinman, A. D.; Thorne, K.; Anseth, K. S. Delivery of osteoinductive growth factors from degradable PEG hydrogels influences osteoblast differentiation and mineralization. *J. Controlled Release* **2002**, *83* (1), 53−63.

(31) Sun, J.; Jiao, L.; Wei, X.; Peng, W.; Liu, L.; Yuan, H. Effect of PEG molecular weight on the crystal structure and electrochemical performance of LiV 3 O 8. *J. Solid State Electrochem.* **2010**, *14* (4), 615−619.

(32) Xie, A.-J.; Zhang, C.-Y.; Shen, Y.-H.; Qiu, L.-G.; Xiao, P.-P.; Hu, Z.-Y. Morphologies of calcium carbonate crystallites grown from aqueous solutions containing polyethylene glycol. *Cryst. Res. Technol.* **2006**, *41* (10), 967−971.

(33) Liu, D.; Yang, Q.; Troczynski, T. Sol-gel hydroxyapatite coatings on stainless steel substrates. *Biomaterials* **2002**, *23* (3), 691−698.

(34) Kim, I.; Kumta, P. Sol-gel synthesis and characterization of nanostructured hydroxyapatite powder. *Mater. Sci. Eng. B* **2004**, *111* (2−3), 232−236.

(35) Han, Y.; Li, S.; Wang, X.; Chen, X. Synthesis and sintering of nanocrystalline hydroxyapatite powders by citric acid sol-gel combustion method. *Mater. Res. Bull.* **2004**, *39* (1), 25−32.

(36) Cho, J.; Jung, D.; Han, J.; Kang, Y. Spherical shape hydroxyapatite powders prepared by flame spray pyrolysis. *J. Ceram. Process. Res.* **2008**, *9* (4), 348−352.

(37) Yeong, K.; Wang, J.; Ng, S. Mechanochemical synthesis of nanocrystalline hydroxyapatite from CaO and CaHPO4. *Biomaterials* **2001**, *22* (20), 2705−2712.

(38) Rhee, S. Synthesis of hydroxyapatite via mechanochemical treatment. *Biomaterials* **2002**, *23* (4), 1147−1152.

(39) Toriyama, M.; Ravaglioli, A.; Krajewski, A.; Celotti, G.; Piancastelli, A. Synthesis of hydroxyapatite-based powders by mechano-chemical method and their sintering. *J. Eur. Ceram. Soc.* **1996**, *16* (4), 429−436.

(40) Shuk, P.; Suchanek, W.; Hao, T.; Gulliver, E.; Riman, R.; Senna, M.; TenHuisen, K.; Janas, V. Mechanochemical-hydrothermal preparation of crystalline hydroxyapatite powders at room temperature. *J. Mater. Res.* **2001**, *16* (5), 1231−1234.

(41) Suchanek, W.; Byrappa, K.; Shuk, P.; Riman, R.; Janas, V.; TenHuisen, K. Preparation of magnesium-substituted hydroxyapatite powders by the mechanochemical-hydrothermal method. *Biomaterials* **2004**, *25* (19), 4647−4657.

(42) Diegmueller, J. J.; Cheng, X.; Akkus, O. Modulation of Hydroxyapatite Nanocrystal Size and Shape by Polyelectrolytic Peptides. *Cryst. Growth Des.* **2009**, *9* (12), 5220−5226.

(43) Byrappa, K.; Yoshimura, M. *Handbook of Hydrothermal Technology—A Technology for Crystal Growth and Materials Processing*; William Andrew Publishing/Noyes: Norwich , NY, 2001.

(44) Lin, K.; Chang, J.; Cheng, R.; Ruan, M. Hydrothermal microemulsion synthesis of stoichiometric single crystal hydroxyapatite

nanorods with mono-dispersion and narrow-size distribution. *Mater. Lett.* **2007**, *61* (8−9), 1683−1687.
(45) Cai, Y.; Liu, Y.; Yan, W.; Hu, Q.; Tao, J.; Zhang, M.; Shi, Z.; Tang, R. Role of hydroxyapatite nanoparticle size in bone cell proliferation. *J. Mater. Chem.* **2007**, *17* (36), 3780−3787.
(46) Zhang, H.; Zhang, M. Phase and thermal stability of hydroxyapatite whiskers precipitated using amine additives. *Ceram. Int.* **2011**, *37* (1), 279−286.
(47) Cao, L.; Li, L.; Zhang, P.; Wu, H. Influence of CaF 2 on the structure and dielectric properties of Ag (Nb 0.8 Ta 0.2) O 3 ceramics. *Rare Met.* **2010**, *29* (1), 50−54.
(48) Horikoshi, K.; Hata, K.; Kawabata, N.; Ikawa, S.-I.; Konaka, S. Vibrational spectra and conformation of polyethylene glycol complexed with calcium and magnesium chlorides. *J. Mol. Struct.* **1990**, *239* (0), 33−42.
(49) Chen, J. D.; Wang, Y. J.; Wei, K.; Zhang, S. H.; Shi, X. T. Self-organization of hydroxyapatite nanorods through oriented attachment. *Biomaterials* **2007**, *28* (14), 2275−2280.
(50) Rapacz-Kmita, A.; Paluszkiewicz, C.; Ślósarczyk, A.; Paszkiewicz, Z. FTIR and XRD investigations on the thermal stability of hydroxyapatite during hot pressing and pressureless sintering processes. *J. Mol. Struct.* **2005**, *744−747* (0), 653−656.
(51) Vignoles, M.; Bonel, G.; Holcomb, D.; Young, R. Influence of preparation conditions on the composition of type B carbonated hydroxyapatite and on the localization of the carbonate ions. *Calcif. Tissue Int.* **1988**, *43* (1), 33−40.
(52) Barralet, J.; Best, S.; Bonfield, W. Carbonate substitution in precipitated hydroxyapatite: An investigation into the effects of reaction temperature and bicarbonate ion concentration. *J. Biomed. Mater. Res.* **1998**, *41* (1), 79−86.
(53) Osman, I.; Seyfullah, K.; Burcu, C. The Effect of PEG on the Water Absorption Capacity and Rate of Superabsorbent Copolymers Based on Acrylic Acid. *Int. J. Polym. Mater.* **2005**, *54* (11), 1001−1008.
(54) Kumta, P. N.; Sfeir, C.; Lee, D.-H.; Olton, D.; Choi, D. Nanostructured calcium phosphates for biomedical applications: Novel synthesis and characterization. *Acta Biomater.* **2005**, *1* (1), 65−83.
(55) Wang, P. E.; Chaki, T. Sintering behaviour and mechanical properties of hydroxyapatite and dicalcium phosphate. *J. Mater. Sci.: Mater. Med.* **1993**, *4* (2), 150−158.
(56) Weng, J.; Liu, X.; Zhang, X.; Ji, X. Thermal decomposition of hydroxyapatite structure induced by titanium and its dioxide. *J. Mater. Sci. Lett.* **1994**, *13* (3), 159−161.
(57) Loher, S.; Stark, W. J.; Maciejewski, M.; Baiker, A.; Pratsinis, S. E.; Reichardt, D.; Maspero, F.; Krumeich, F.; Günther, D. Fluoro-apatite and calcium phosphate nanoparticles by flame synthesis. *Chem. Mater.* **2005**, *17* (1), 36−42.
(58) Loo, S. C. J.; Siew, Y. E.; Ho, S.; Boey, F. Y. C.; Ma, J. Synthesis and hydrothermal treatment of nanostructured hydroxyapatite of controllable sizes. *J. Mater. Sci.: Mater. Med.* **2008**, *19* (3), 1389−1397.
(59) Aguilar-Frutis, M.; Kumar, S.; Falcony, C. Spray-pyrolyzed hydroxyapatite thin-film coatings. *Surf. Coat. Technol.* **2009**, *204* (6−7), 1116−1120.
(60) Guo, X.; Xiao, P. Effects of solvents on properties of nanocrystalline hydroxyapatite produced from hydrothermal process. *J. Eur. Ceram. Soc.* **2006**, *26* (15), 3383−3391.
(61) Kothapalli, C. R.; Wei, M.; Legeros, R. Z.; Shaw, M. T. Influence of temperature and aging time on HA synthesized by the hydrothermal method. *J. Mater. Sci.: Mater. Med.* **2005**, *16* (5), 441−446.
(62) Kay, M. I.; Young, R. A.; Posner, A. S. Crystal Structure of Hydroxyapatite. *Nature* **1964**, *204* (4963), 1050−1052.
(63) Qiu, C. F.; Xiao, X. F.; Liu, R. F.; She, H. D. Biomimetic synthesis of spherical nano-hydroxyapatite with polyvinylpyrrolidone as template. *Mater. Sci. Technol.* **2008**, *24* (5), 612−617.
(64) Wang, Y.; Zhang, S.; Wei, K.; Zhao, N.; Chen, J.; Wang, X. Hydrothermal synthesis of hydroxyapatite nanopowders using cationic surfactant as a template. *Mater. Lett.* **2006**, *60* (12), 1484−1487.
(65) Uota, M.; Arakawa, H.; Kitamura, N.; Yoshimura, T.; Tanaka, J.; Kijima, T. Synthesis of High Surface Area Hydroxyapatite Nano-particles by Mixed Surfactant-Mediated Approach. *Langmuir* **2005**, *21* (10), 4724−4728.